

DISCRIMINATING THE PROGENITOR TYPE OF SUPERNOVA REMNANTS  
WITH IRON K-SHELL EMISSIONHIROYA YAMAGUCHI<sup>1,2,3</sup>, CARLES BADENES<sup>4</sup>, ROBERT PETRE<sup>1</sup>, TOSHIO NAKANO<sup>5</sup>, DANIEL CASTRO<sup>6</sup>,  
TERUAKI ENOTO<sup>1,7</sup>, JUNKO S. HIRAGA<sup>5</sup>, JOHN P. HUGHES<sup>8</sup>, YOSHITOMO MAEDA<sup>9</sup>, MASAYOSHI NOBUKAWA<sup>10</sup>,  
SAMAR SAFI-HARB<sup>11,12</sup>, PATRICK O. SLANE<sup>3</sup>, RANDALL K. SMITH<sup>3</sup>, HIROYUKI UCHIDA<sup>10</sup>*Draft version February 28, 2024*

## ABSTRACT

Supernova remnants (SNRs) retain crucial information about both their parent explosion and circumstellar material left behind by their progenitor. However, the complexity of the interaction between supernova ejecta and ambient medium often blurs this information, and it is not uncommon for the basic progenitor type (Ia or core-collapse) of well-studied remnants to remain uncertain. Here we present a powerful new observational diagnostic to discriminate between progenitor types and constrain the ambient medium density of SNRs solely using Fe K-shell X-ray emission. We analyze all extant *Suzaku* observations of SNRs and detect Fe K $\alpha$  emission from 23 young or middle-aged remnants, including five first detections (IC 443, G292.0+1.8, G337.2–0.7, N49, and N63A). The Fe K $\alpha$  centroids clearly separate progenitor types, with the Fe-rich ejecta in Type Ia remnants being significantly less ionized than in core-collapse SNRs. Within each progenitor group, the Fe K $\alpha$  luminosity and centroid are well correlated, with more luminous objects having more highly ionized Fe. Our results indicate that there is a strong connection between explosion type and ambient medium density, and suggest that Type Ia supernova progenitors do not substantially modify their surroundings at radii of up to several parsecs. We also detect a K-shell radiative recombination continuum of Fe in W49B and IC 443, implying a strong circumstellar interaction in the early evolutionary phases of these core-collapse remnants.

*Subject headings:* ISM: supernova remnants — ISM: abundances — X-rays: ISM

## 1. INTRODUCTION

Supernova remnants (SNRs) provide unique insights into both the supernova (SN) explosion that generated them and the ambient medium that surrounded their progenitors at the time of the explosion. Unfortunately, the complex physical processes involved in the interaction between ejecta and ambient medium often blur this information, to the point that the explosion type (i.e., Type Ia or core-collapse: Ia and CC hereafter) of several well-studied SNRs still remains controversial.

The X-ray emission from young and middle-aged SNRs is ideally suited to disentangle the contributions from

the SN explosion and circumstellar interaction (see Vink 2012, for a recent review). Their thermal X-ray spectra are often dominated by strong optically-thin emission lines from ejecta that retain the nucleosynthetic signature of their birth events. On the other hand, the X-ray emitting plasma is in a state of non-equilibrium ionization (NEI), and its time-dependent ionization degree is controlled by the ambient medium density, which is a sensitive diagnostic of the presence of circumstellar material (CSM) left behind by the SN progenitor (e.g., Badenes et al. 2005, 2007).

Indeed, much progress has been made in the typing of SNRs using their X-ray emission. Using *ASCA* data, Hughes et al. (1995) showed that it is possible to distinguish Ia remnants from CC ones by virtue of their ejecta composition; Fe-rich and O-poor SNRs are likely Ia, while SNRs dominated by O and Ne lines with weak Fe L emission are likely CC. More recently, Lopez et al. (2009, 2011) argued that *Chandra* images of Ia SNRs show a higher degree of symmetry than those of CC SNRs. This result implies that CC SNe are more asymmetric than Ia SNe, and/or CC SNRs expand into more asymmetric CSM. These methods are promising, but require sophisticated analysis techniques whose results might lead to ambiguous interpretations. Abundance determination in NEI plasmas is notoriously uncertain (see Borkowski et al. 2001, for a discussion), and neither of these methods easily leads to placement of quantitative constraints on the presence of CSM in a SNR. In this *Letter*, we present a new, straightforward observational diagnostic for typing SNRs in X-rays that relies only on the centroid and flux of a single spectral line – the Fe K $\alpha$  emission at 6.4–6.7 keV.

The Fe K line blend is well separated from emission

Electronic address: hiroya.yamaguchi@nasa.gov

<sup>1</sup> NASA Goddard Space Flight Center, Code 662, Greenbelt, MD 20771, USA

<sup>2</sup> Department of Astronomy, University of Maryland, College Park, MD 20742, USA

<sup>3</sup> Harvard-Smithsonian Center for Astrophysics, 60 Garden Street, Cambridge, MA 02138, USA

<sup>4</sup> Department of Physics and Astronomy and Pittsburgh Particle Physics, Astrophysics and Cosmology Center (PITT PACC), University of Pittsburgh, 3941 O'Hara St, Pittsburgh, PA 15260, USA

<sup>5</sup> Department of Physics, The University of Tokyo, Bunkyo, Tokyo, 113-0033, Japan

<sup>6</sup> MIT-Kavli Center for Astrophysics and Space Research, 77 Massachusetts Avenue, Cambridge, MA 02139, USA

<sup>7</sup> RIKEN (The Institute of Physical and Chemical Research), 2-1 Hirosawa, Wako, Saitama 351-0198, Japan

<sup>8</sup> Department of Physics and Astronomy, Rutgers University, 136 Frelinghuysen Road, Piscataway, NJ 08854, USA

<sup>9</sup> Institute of Space and Astronautical Science, JAXA, 3-1-1 Yoshinodai, Sagami-hara, Kanagawa 229-8510, Japan

<sup>10</sup> Department of Physics, Kyoto University, Kitashirakawa-oiwake-cho, Sakyo-ku, Kyoto 606-8502, Japan

<sup>11</sup> Department of Physics and Astronomy, University of Manitoba, Winnipeg, MB R3T 2N2, Canada

<sup>12</sup> Canada Research Chair

lines of other abundant elements. Since the production of Fe occurs at the heart of an SN explosion, reverse shock heating of this element can be delayed compared to elements synthesized in the outer layers. This often results in an ionization state lower than He-like ( $\text{Fe}^{24+}$ ) in young or middle-aged SNRs. The ionization state in turn determines the Fe  $K\alpha$  centroid (e.g., Yamaguchi et al. 2014), which is easily measured using current CCD instruments. Furthermore, the Fe K emission is largely unaffected by foreground extinction, unlike Fe L-shell blends. These spectral advantages and simplicities make our method more straightforward than the existing ones, and especially attractive for current and future X-ray missions with high throughput, like *Suzaku*, *XMM-Newton*, and *Astro-H*. Here we show that the Fe  $K\alpha$  centroids (hence the Fe ionization state) clearly discriminate the progenitor type and place strong limits on the presence of CSM in SNRs at radii of several parsecs, which has important consequences for SN progenitor studies.

## 2. DATA ANALYSIS

We analyzed archival data of all SNRs that *Suzaku* has observed to date with the X-ray Imaging Spectrometer (XIS), with no bias nor specific selection criterion. To search for Fe  $K\alpha$  emission, we extracted XIS spectra from the entire X-ray emitting region of each SNR. The only exception was IC 443, which because of its large angular size was only partially imaged by the XIS. For this SNR, we extracted the spectrum from a  $10'$ -diameter circular region in the brightest northern part, and estimated the Fe  $K\alpha$  flux from the whole SNR by scaling the surface brightness using archival *XMM-Newton* data. Background subtraction was performed in the following manner: (1) If nearby blank sky data with taken using an identical detector operating mode were available, we used them to extract a background spectrum from the same detector region as the source. (2) If the SNR angular size is small enough ( $d \lesssim 10'$ ) compared with the XIS field of view, background data were taken from the surrounding region. (3) Otherwise, we subtracted only the instrumental background component (NXB; simulated by the `xisnxbgen` task), and included models for the extragalactic background (a.k.a. CXB) and Galactic Ridge X-ray emission (GRXE) in our analysis. To estimate the GRXE flux, we followed the relationship between surface brightness and Galactic coordinates described by Uchiyama et al. (2013). As a consistency check, we applied method (3) to all the SNRs which satisfied the criteria for methods (1) and (2), and found no significant change in the measured Fe  $K\alpha$  blend parameters.

We detected Fe  $K\alpha$  emission from the 23 SNRs listed in Table 1, including five first detections: G337.2-0.7, IC 443, G292.0+1.8, N49, and N63A. SNRs without detectable Fe  $K\alpha$  emission can be categorized in two groups: evolved SNRs whose electron temperature is too low ( $\lesssim 1$  keV) to excite K-shell transitions in Fe atoms, and young SNRs where the hard X-ray spectrum is dominated by a strong nonthermal continuum. The former category includes most interstellar medium-dominated SNRs (e.g., Cygnus Loop, G156.2+5.7, DEM L71), while the latter includes both shell-like SNRs with cosmic-ray-accelerating blast waves (e.g., G1.9+0.3, RX J1713.7-3946) and plerionic SNRs (e.g., Crab, G21.5-0.9). Recent *Chandra* observations of G1.9+0.3 separated spa-

tially the thermal emission from the nonthermal continuum, and enabled the detection of Fe  $K\alpha$  emission (Borkowski et al. 2010, 2013). Although *Suzaku* observed this SNR for  $\sim 100$  ks, the Fe  $K\alpha$  emission was not spatially resolved and remained undetected. A few SNRs located near the Galactic plane (e.g., G272.2-3.2, Kes 27) showed hints of Fe  $K\alpha$  emission in their NXB-subtracted spectra, but the fluxes were not significantly larger than those predicted for the GRXE background, so we excluded them from our study.

We fitted the 5–10 keV spectrum of each SNR with a power-law (or bremsstrahlung) continuum plus a Gaussian for Fe  $K\alpha$  emission. Foreground absorption columns are given in Table 1. Some SNRs show emission from Cr, Mn, and/or Ni, and higher transition series of Fe K emission, which were modeled using additional Gaussians. A radiative recombination continuum (RRC) of Fe XXV was detected in W49B and IC 443. We modeled this component with an exponential function with a threshold energy of 8.8 keV (corresponding to the ionization potential of  $\text{Fe}^{24+}$ , following Ozawa et al. (2009). This is the first detection of the Fe RRC from IC 443, indicating that Fe atoms in this remnant are significantly overionized, similar to Si and S (Yamaguchi et al. 2009). The result is presented in more detail in a separate paper (Ohnishi et al. 2014). We list the measured centroid energy and unabsorbed flux of the Fe  $K\alpha$  blend for each SNR in Table 1.

## 3. DISCUSSION

Figure 1 shows the Fe  $K\alpha$  centroid energy and line luminosity for each SNR, together with the corresponding effective charge state  $\langle z_{\text{Fe}} \rangle$  (Yamaguchi et al. 2014). The line luminosities were calculated from the derived unabsorbed fluxes using the distances given in Table 1. The uncertainty in distance to the Galactic SNRs is assumed to be  $\pm 10\%$  of the mean values. Although some sources have larger uncertainties (e.g., G349.7+0.2, see Tian & Leahy 2014), the fundamental result is not affected, since the line centroids play a more important role than the luminosities in typing SNRs as described below. Also shown in Figure 1 are theoretical predictions for SNR models derived from Chandrasekhar-mass Type Ia SN ejecta profiles evolving in a uniform ambient medium density in the range of  $(1-5) \times 10^{-24} \text{ g cm}^{-3}$  for SNR ages of up to 5000 yrs (see Badenes et al. 2003, 2005, 2006, for details on the models). The ejecta profiles shown include three delayed detonation explosion models spanning the nominal range of SN Ia kinetic energies and  $^{56}\text{Ni}$  yields (DDTa, DDTc, and DDTg), and two pulsating delayed detonation explosions (PDDa and PDDc). The predicted Fe  $K\alpha$  centroids and luminosities are calculated using updated atomic data (Yamaguchi et al. 2014). The efficiency of collisionless electron heating at the reverse shock is set so that the electron-to-ion temperature ratio is 0.01–0.03 at the immediate post-shock region (Badenes et al. 2005; Yamaguchi et al. 2014). Similar models for CC SNRs are not available in the literature, but the Ia SNR models and the distribution of the data points in Figure 1 allow us to make a number of important interpretations using our SNR sample.

First, all *bona fide* Ia SNRs have an Fe  $K\alpha$  centroid of  $\lesssim 6550$  keV ( $\langle z_{\text{Fe}} \rangle \lesssim 20$ ), while all *bona fide* CC SNRs have a higher centroid energy. The separation

**Table 1**  
List of the SNRs where Fe-K $\alpha$  emission is detected.<sup>a</sup>

| Name <sup>b</sup>                 | Obs. ID       | Exposure<br>(ks) | Energy<br>(eV)     | Photon Flux<br>( $10^{-5} \text{ cm}^{-2} \text{ s}^{-1}$ ) | $N_{\text{H}}^c$<br>( $10^{22} \text{ cm}^{-2}$ ) | Distance<br>(kpc) | Radius<br>(pc) | Age<br>(yr) | BGD <sup>d</sup> | Refs. |
|-----------------------------------|---------------|------------------|--------------------|---|---|-------------------|----------------|-------------|------------------|-------|
| Type Ia SNRs and candidates       |               |                  |                    |   |   |                   |                |             |                  |       |
| Kepler                            | 5050920[1–7]0 | 574              | $6438 \pm 1$       | $34.6 \pm 0.2$  | 0.5   | 4.8               | 2.4            | 410         | (1)              | 1     |
| 3C 397 <sup>†</sup>               | 505008010     | 69               | $6556^{+4}_{-3}$   | $13.7 \pm 0.4$  | 3.0   | 10.3              | 10.5           | 1500–5500   | (2)              | 2,3   |
| Tycho*                            | 5030850[1,2]0 | 416              | $6431 \pm 1$       | $61.0 \pm 0.4$  | 0.7   | 2.8               | 3.4            | 442         | (2)              | 4,5   |
| RCW 86 <sup>†</sup>               | (See Note)    | 378              | $6408^{+4}_{-5}$   | $14.0 \pm 0.7$  | 0.3   | 2.5               | 16             | 1829        | (3)              | 6     |
| SN 1006*                          | (See Note)    | 317              | $6429 \pm 10$      | $2.55 \pm 0.43$   | 0.07  | 2.2               | 10             | 1008        | (3)              | 7     |
| G337.2–0.7                        | 507068010     | 304              | $6505^{+26}_{-31}$ | $0.21 \pm 0.06$   | 4.0   | 9.3               | 8.1            | 5000–7000   | (2)              | 8     |
| G344.7–0.1 <sup>†</sup>           | 501011010     | 42               | $6463^{+9}_{-10}$  | $4.03 \pm 0.33$   | 5.0   | 14                | 16             | 3000–6000   | (2)              | 9     |
| G352.7–0.1 <sup>†</sup>           | 506052010     | 202              | $6443^{+8}_{-12}$  | $0.82 \pm 0.08$   | 2.6   | 7.5               | 6.0            | ~5000       | (2)              | 10    |
| N103B <sup>†</sup>                | 804039010     | 224              | $6545 \pm 6$       | $2.15 \pm 0.10$   | 0.06  | 50                | 3.6            | ~860        | (2)              | 11,12 |
| 0509–67.5*                        | 5080720[1,2]0 | 329              | $6425^{+14}_{-15}$ | $0.32 \pm 0.04$   | 0.05  | 50                | 3.6            | ~400        | (2)              | 12,13 |
| 0519–69.0*                        | 806026010     | 348              | $6498^{+6}_{-8}$   | $0.93 \pm 0.05$   | 0.06  | 50                | 4.0            | ~600        | (2)              | 12,14 |
| Core-collapse SNRs and candidates |               |                  |                    |   |   |                   |                |             |                  |       |
| Sgr A East*                       | (See Note)    | 88               | $6664 \pm 3$       | $22.3 \pm 1.0$  | 10  | 8.5               | 3.7            | ~4000       | (2)              | 15    |
| G0.61+0.01 <sup>†</sup>           | 100037060     | 77               | $6634^{+14}_{-12}$ | $3.3 \pm 0.5$   | 16  | 8.5               | 5.0            | ~7000       | (2)              | 16    |
| W49B                              | 50308[4,5]010 | 114              | $6663 \pm 1$       | $109 \pm 1$   | 5.0   | 8.0               | 5.8            | 1000–3000   | (2)              | 17    |
| Cas A*                            | 100043020     | 7                | $6617^{+3}_{-2}$   | $435 \pm 9$   | 2.0   | 3.4               | 2.7            | 310–350     | (2)              | 18    |
| IC 443                            | 5070150[1–4]0 | 368              | $6674^{+10}_{-13}$ | $6.01 \pm 0.59$   | 0.6   | 1.5               | 10             | 4000–30000  | (3)              | 19    |
| G292.0+1.8*                       | 506062010     | 44               | $6585^{+27}_{-28}$ | $1.38 \pm 0.35$   | 0.5   | 6.2               | 11             | ~3000       | (3)              | 20    |
| G349.7+0.2                        | 506064010     | 160              | $6617^{+7}_{-6}$   | $2.92 \pm 0.18$   | 7.0   | 11.5              | 4.0            | ~3500       | (2)              | 21,22 |
| G350.1–0.3*                       | 506065010     | 70               | $6587^{+11}_{-10}$ | $2.24 \pm 0.23$   | 3.7   | 4.5               | 1.3            | ~900        | (2)              | 23    |
| N49 <sup>†</sup>                  | 807007010     | 185              | $6628^{+29}_{-26}$ | $0.18 \pm 0.04$   | 0.06  | 50                | 8.5            | ~6600       | (2)              | 24    |
| N63A                              | 508071010     | 82               | $6647^{+16}_{-17}$ | $0.86 \pm 0.12$   | 0.06  | 50                | 10             | 2000–5000   | (2)              | 25    |
| N132D                             | (See Note)    | 86               | $6656 \pm 9$       | $1.83 \pm 0.17$   | 0.06  | 50                | 13             | ~3150       | (2)              | 26    |
| SN 1987A*                         | 707020010     | 81               | $6646^{+55}_{-54}$ | $0.19 \pm 0.08$   | 0.06  | 50                | 0.2            | 27          | (2)              | 27    |

**Note.** — <sup>a</sup>The uncertainties are in the 90% confidence range.

<sup>b</sup>The asterisks (\*) indicate the SNRs for which classification is robust from a known association to a compact object, light echo spectroscopy, and/or detailed modeling of the ejecta emission. The daggers (†) indicate that the progenitor type of these SNRs is controversial or unknown.

<sup>c</sup>Absorption column density with the solar elemental composition (Wilms et al. 2000). For the LMC SNRs, only the Galactic component (Dickey & Lockman 1990) is shown, but the absorption in the LMC ( $\lesssim 10^{21} \text{ cm}^{-2}$ ) does not affect the spectra above 5 keV.

<sup>d</sup>Background subtraction method we applied (see text in §2).

**Observation ID** — RCW 86: 503004010, 501037010, 503001010, 503002010, 503003010, 503004010 — SN 1006: 500016010, 500017010, 502046010 — Sgr A East: 100027010, 100037040, 100048010 — N132D: 105011010, 106010010, 106010020

**Representative references** — (1) Reynolds et al. (2007); (2) Chen et al. (1999); (3) Safi-Harb et al. (2005); (4) Badenes et al. (2006); (5) Tian & Leahy (2011); (6) Williams et al. (2011); (7) Yamaguchi et al. (2008); (8) Rakowski et al. (2006); (9) Yamaguchi et al. (2012); (10) Giacani et al. (2009); (11) Lewis et al. (2003); (12) Rest et al. (2005); (13) Warren & Hughes (2004); (14) Kosenko et al. (2010); (15) Koyama et al. (2007a); (16) Koyama et al. (2007b); (17) Keohane et al. (2007); (18) Hwang & Laming (2012); (19) Troja et al. (2008); (20) Park et al. (2004); (21) Lazendic et al. (2005); (22) Tian & Leahy (2014); (23) Gaensler et al. (2008); (24) Park et al. (2012); (25) Warren et al. (2003); (26) Borkowski et al. (2007); (27) Maggi et al. (2012)

is very clear: no single object with a robust progenitor type (i.e., from a known association to a compact object, or light echo spectroscopy, or detailed modeling of the ejecta emission) falls on the wrong side of the centroid boundary. Since the Ia and CC SNRs in our sample have similar ages and radii, this large difference in the ionization state must be due to significantly higher ambient medium densities in the CC SNRs. This is in line with the expectations from stellar evolution models, which predict significant (several  $M_{\odot}$ ) mass loss from CC SN progenitors, either due to winds or binary evolution (Langer 2012). In any case, the clear division in Fe K $\alpha$  centroid allows us to firmly establish the classification of several objects with unclear or controversial types. Both RCW 86 and G344.7–0.1 were once considered to be CC SNRs (e.g., Vink et al. 1997; Lopez et al. 2011), but recent observations have suggested a Ia origin (e.g., Williams et al. 2011; Yamaguchi et al. 2012). The latter is supported by our study. The Fe K $\alpha$  centroid of the Ia SNR G337.2–0.7 (Rakowski et al. 2006)

falls a bit outside the range of our theoretical models, but this is not surprising given the estimated age (5000–7000 yr). Giacani et al. (2009) suggested that the highly absorbed SNR G352.7–0.1 might have been a CC event, but its Fe K $\alpha$  centroid puts it squarely in the Ia region. The Fe K $\alpha$  centroid for G1.9+0.3 reported by Borkowski et al. (2013) also falls within the Ia region, supporting the typing of this SNR by Borkowski et al. (2010). Likewise, several SNRs suspected to be of a CC origin without confirmed associations with compact objects (e.g., G0.61+0.01: Koyama et al. 2007b; N49: Park et al. 2012; N63A: Warren et al. 2003; N132D: Borkowski et al. 2007) fall clearly in the CC region due to their high centroid energies. From the Fe K $\alpha$  centroid alone, the classification for 3C 397 and N103B is somewhat unclear. We emphasize, however, that the observed Fe K $\alpha$  parameters of both SNRs can be well reproduced by our Ia SNR models. If 3C 397 is indeed a Type Ia remnant (as suggested by Chen et al. 1999), it should be relatively old ( $\gtrsim 3000$  yr) and has evolved in a high density

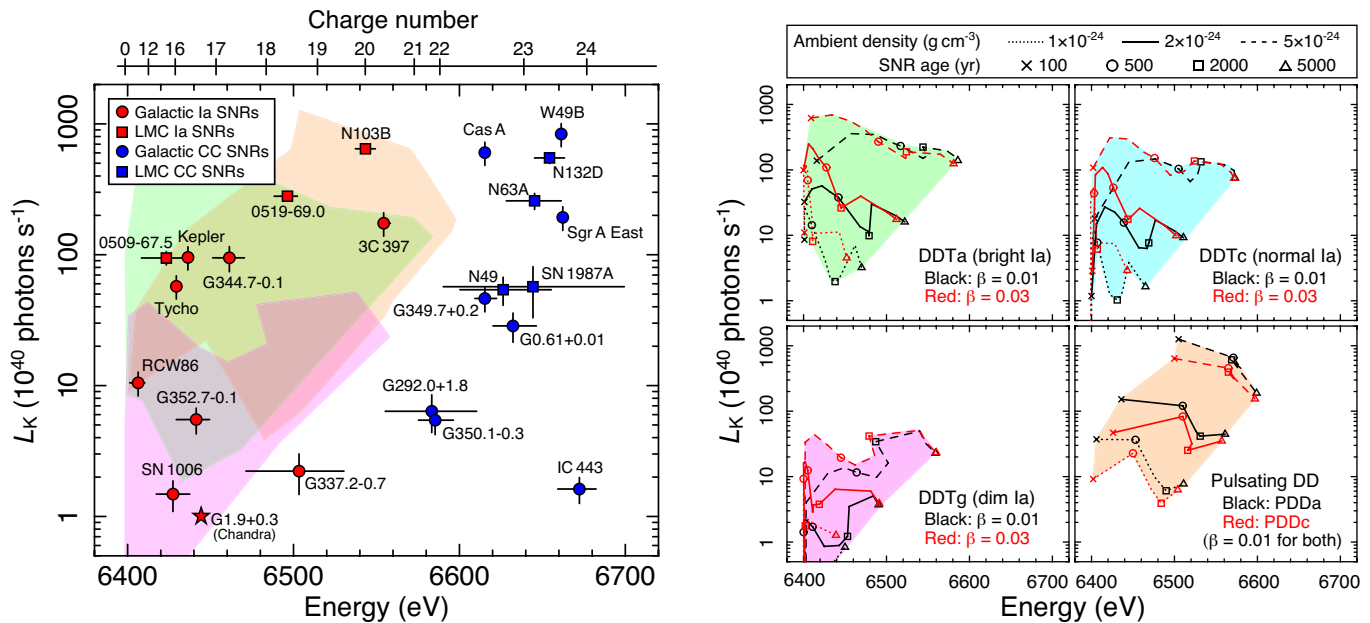


**Figure 1.** *Left:* Centroid energies and line luminosities of Fe K $\alpha$  emission from various SNRs in our Galaxy (circles) and the LMC (squares). The corresponding effective charge number is given above the panel. Red and blue represent Ia and CC SNRs or their candidates, respectively. The mean centroid and luminosity of Fe K $\alpha$  emission from G1.9+0.3 observed by *Chandra* (Borkowski et al. 2013) are also indicated with the red star. The shaded regions represent the Fe K $\alpha$  centroids and luminosities predicted by the theoretical Type Ia SNR models (DDTa: green, DDTg: magenta, PDD: orange; see right panel for details). *Right:* Predicted Fe K $\alpha$  parameters for the various models of Type Ia SNRs evolving in a uniform ambient medium densities of  $1 \times 10^{-24} \text{ g cm}^{-3}$  (dotted),  $2 \times 10^{-24} \text{ g cm}^{-3}$  (solid), and  $5 \times 10^{-24} \text{ g cm}^{-3}$  (dashed). Crosses, circles, squares and triangles indicate SNR ages of 100 yr, 500 yr, 2000 yr, and 5000 yr, respectively.

interstellar medium ( $\sim 5 \times 10^{-24} \text{ g cm}^{-3}$ ), given the comparison with our model plots. These values are consistent with the estimates of Safi-Harb et al. (2005), although a CC origin was suggested in their work. The explosion type of N103B has also been a matter of controversy (e.g., van der Heyden et al. 2002; Lewis et al. 2003), but we favor the Ia hypothesis, based on the high maximum luminosity of its parent explosion inferred from the light echo data (Rest et al. 2005), in addition to the properties of the Fe K $\alpha$  emission.

Second, within each group, the centroids and line luminosities are fairly well correlated, such that SNRs with more highly ionized Fe tend to have more luminous Fe K $\alpha$  lines. This is likely a consequence of the NEI characteristics of the emitting plasma; in order to collisionally ionize Fe atoms to higher states, higher post-shock densities are required, which also result in higher emission measures and thus X-ray luminosities. The SNR age also plays a role in the ionization state of the ejecta, but ambient medium density is the main driver, as illustrated by the Ia SNR models in Figure 1. Interestingly, both SNR types span a similar range of Fe K $\alpha$  luminosities, despite the fact that typical ejected mass of Fe ( $^{56}\text{Ni}$ ) is an order of magnitude smaller in CC than in Ia SNe (Woosley & Weaver 1995; Iwamoto et al. 1999). This is again due to the higher emission measure associated with higher post shock density, and is one of the reasons why typing SNRs has been difficult without having a detailed model for their dynamics and plasma evolution. In this context, the relatively high Fe K $\alpha$  centroid and luminosity for SN 1987A are particularly interesting, given the young age and low ejected Fe mass of this SNR. The progenitors of the overionized SNRs, W49B and IC 443,

might have an especially high mass loss rate, leading to a CSM dense enough to produce a strong circumstellar interaction in the early evolutionary phase of their remnants (e.g., Yamaguchi et al. 2009).

Finally, although our Ia SNR models are relatively simplistic (one-dimensional hydrodynamics in uniform ambient density), the parameter space they span includes *all* Ia SNRs. This is remarkable in its own right, because some Ia SNRs, like Kepler (Reynolds et al. 2007) and N103B (Lewis et al. 2003), are known to be interacting with a nonuniform ambient medium. Our analysis does not rule out the presence of CSM in these objects, but simply indicates that deviations from a uniform ambient medium in Ia SNRs, if present, cannot be very large, and rules out large CSM masses (several  $M_{\odot}$ ) as seen in CC SNRs. Middle-aged Ia SNRs with low Fe K $\alpha$  centroids and luminosities might be interacting with an exceptionally low density interstellar medium (e.g., SN1006: Yamaguchi et al. 2008), or with a low-density wind-blown cavity excavated by the progenitor (e.g., RCW 86: Williams et al. 2011). On the other hand, young Ia SNRs with higher Fe K $\alpha$  centroids and luminosities, like N103B (Lewis et al. 2003), might be interacting with some kind of CSM, but their Fe K $\alpha$  emission can also be explained by uniform ambient density models, at least at the level of detail allowed by our study.

#### 4. CONCLUSIONS

We have presented a systematic analysis of Fe K $\alpha$  emission from 23 Galactic and LMC SNRs observed by *Suzaku*. We find that the Fe K $\alpha$  line luminosities of Type Ia and CC SNRs are distributed in a similar range ( $L_K$



$= 10^{40-43}$  photons  $s^{-1}$ ), but the Fe  $K\alpha$  centroid energies clearly distinguish Ia from CC SNRs, with the former always having centroids below  $\sim 6.55$  keV and the latter always above. We interpret this separation as a signature of different mass-loss rates in Ia and CC SN progenitors. The Fe  $K\alpha$  emission of all the Ia objects in our sample is compatible with SNR models that expand into a uniform ambient medium, which suggests that Ia progenitors do not modify their surroundings as strongly as CC progenitors do. This is in line with known limits from prompt X-ray (Hughes et al. 2007) and radio (Chomiuk et al. 2012) emission from Ia SNe, but our results probe a different regime, constraining the structure of the CSM to larger radii (several pc) and progenitor mass loss rates further back in the pre-SN evolution of the progenitor. A quantification of these constraints and a more detailed analysis of the CC SNR sample are left for future work.

The full potential of our method will be realized when it is applied to larger samples of higher quality data, as will be accessible to high resolution spectrometers like those on *Astro-H* and other future missions with large effective areas in the Fe  $K\alpha$  band like *Athena*. These instruments will open the possibility of studying statistically significant samples of X-ray emitting SNRs in nearby galaxies with resolved stellar populations like M31, which will in turn dramatically increase our knowledge of both Type Ia and CC SN progenitors.

We are grateful to Dr. Katsuji Koyama for providing *Suzaku* data he obtained as a Principal Investigator and kindly reviewing our manuscript. We also thank Drs. Kazimierz J. Borkowski, Thomas M. Dame, Adam, R. Foster, John D. Raymond, Satoru Katsuda, Toshiaki Sato, and Hideki Uchiyama for helpful discussion and suggestions in preparing this paper.

## REFERENCES

- Badenes, C., Bravo, E., Borkowski, K. J., & Domínguez, I. 2003, *ApJ*, 593, 358
- Badenes, C., Borkowski, K. J., & Bravo, E. 2005, *ApJ*, 624, 198
- Badenes, C., Borkowski, K. J., Hughes, J. P., Hwang, U., & Bravo, E. 2006, *ApJ*, 645, 1373
- Badenes, C., Hughes, J. P., Bravo, E., & Langer, N. 2007, *ApJ*, 662, 472
- Borkowski, K. J., Lyerly, W. J., & Reynolds, S. P. 2001, *ApJ*, 548, 820
- Borkowski, K. J., Hendrick, S. P., & Reynolds, S. P. 2007, *ApJ*, 671, L45
- Borkowski, K. J., Reynolds, S. P., Green, D. A., et al. 2010, *ApJ*, 724, L161
- Borkowski, K. J., Reynolds, S. P., Hwang, U., et al. 2013, *ApJ*, 771, L9
- Chen, Y., Sun, M., Wang, Z.-R., & Yin, Q. F. 1999, *ApJ*, 520, 737
- Chomiuk, L., Soderberg, A. M., Moe, M., et al. 2012, *ApJ*, 750, 164
- Dickey, J. M., & Lockman, F. J. 1990, *ARA&A*, 28, 215
- Gaensler, B. M., Tanna, A., Slane, P. O., et al. 2008, *ApJ*, 680, L37
- Giacani, E., Smith, M. J. S., Dubner, G., et al. 2009, *A&A*, 507, 841
- Hughes, J. P., Hayashi, I., Helfand, D., et al. 1995, *ApJ*, 444, L81
- Hughes, J. P., Chugai, N., Chevalier, R., Lundqvist, P., & Schlegel, E. 2007, *ApJ*, 670, 1260
- Hwang, U., & Laming, J. M. 2012, *ApJ*, 746, 130
- Iwamoto, K., Brachwitz, F., Nomoto, K., et al. 1999, *ApJS*, 125, 439
- Keohane, J. W., Reach, W. T., Rho, J., & Jarrett, T. H. 2007, *ApJ*, 654, 938
- Kosenko, D., Helder, E. A., & Vink, J. 2010, *A&A*, 519, A11
- Koyama, K., Uchiyama, H., Hyodo, Y., et al. 2007a, *PASJ*, 59, S237
- Koyama, K., Inui, T., Hyodo, Y., et al. 2007b, *PASJ*, 59, S221
- Langer, N. 2012, *ARA&A*, 50, 107
- Lazendic, J. S., Slane, P. O., Hughes, J. P., Chen, Y., & Dame, T. M. 2005, *ApJ*, 618, 733
- Lewis, K. T., Burrows, D. N., Hughes, J. P., et al. 2003, *ApJ*, 582, 770
- Lopez, L. A., Ramirez-Ruiz, E., Badenes, C., et al. 2009, *ApJ*, 706, L106
- Lopez, L. A., Ramirez-Ruiz, E., Huppenkothen, D., Badenes, C., & Pooley, D. A. 2011, *ApJ*, 732, 114
- Maggi, P., Haberl, F., Sturm, R., & Dewey, D. 2012, *A&A*, 548, L3
- Ohnishi, T., Uchida, H., Tsuru, T. G., et al. 2014, *ApJ*, 784, 74
- Ozawa, M., Koyama, K., Yamaguchi, H., Masai, K., & Tamagawa, T. 2009, *ApJ*, 706, L71
- Park, S., Hughes, J. P., Slane, P. O., et al. 2004, *ApJ*, 602, L33
- Park, S., Hughes, J. P., Slane, P. O., et al. 2012, *ApJ*, 748, 117
- Rakowski, C. E., Badenes, C., Gaensler, B. M., et al. 2006, *ApJ*, 646, 982
- Rest, A., Suntzeff, N. B., Olsen, K., et al. 2005, *Nature*, 438, 1132
- Reynolds, S. P., Borkowski, K. J., Hwang, U., et al. 2007, *ApJ*, 668, L135
- Safi-Harb, S., Dubner, G., Petre, R., Holt, S. S., & Durouchoux, P. 2005, *ApJ*, 618, 321
- Tian, W. W., & Leahy, D. A. 2011, *ApJ*, 729, L15
- Tian, W. W., & Leahy, D. A. 2014, *ApJ*, 783, L2
- Troja, E., Bocchino, F., Miceli, M., & Reale, F. 2008, *A&A*, 485, 777
- Uchiyama, H., Nobukawa, M., Tsuru, T. G., & Koyama, K. 2013, *PASJ*, 65, 19
- van der Heyden, K. J., Behar, E., Vink, J., et al. 2002, *A&A*, 392, 955
- Vink, J., Kaastra, J. S., & Bleeker, J. A. M. 1997, *A&A*, 328, 628
- Vink, J. 2012, *A&A Rev.*, 20, 49
- Warren, J. S., Hughes, J. P., & Slane, P. O. 2003, *ApJ*, 583, 260
- Warren, J. S., & Hughes, J. P. 2004, *ApJ*, 608, 261
- Williams, B. J., Blair, W. P., Blondin, J. M., et al. 2011, *ApJ*, 741, 96
- Wilms, J., Allen, A., & McCray, R. 2000, *ApJ*, 542, 914
- Woosley, S. E., & Weaver, T. A. 1995, *ApJS*, 101, 181
- Yamaguchi, H., Koyama, K., Katsuda, S., et al. 2008, *PASJ*, 60, S141
- Yamaguchi, H., Ozawa, M., Koyama, K., et al. 2009, *ApJ*, 705, L6
- Yamaguchi, H., Tanaka, M., Maeda, K., et al. 2012, *ApJ*, 749, 137
- Yamaguchi, H., Eriksen, K. A., Badenes, C., et al. 2014, *ApJ*, 780, 136